Uplift: The Rhenish Shield—A Case History, K. Fuchs *et al.*, Eds. (Springer-Verlag, Berlin, 1983), pp. 315–331.
15. H. Bijwaard, W. Spakman, E. R. Engdahl, *J. Geophys. Res.* **103**, 30,055 (1998). The global mantle velocity model of Bijwaard *et al.* is based on the *P*, *pP*, and *pwP* travel time data set of E. R. Engdahl *et al.* [*Bull. Seismol. Soc. Am.* **88**, 722 (1998)] and is computed using an irregular cell parameterization which adapts cell sizes to minimize ray sampling differences between adjacent cells. Under most of Europe, grid cells are 60 to 120 km in size. Cell size increases up to 300 km under the Atlantic and northern Africa. The tomographic model is supported by synthetic tests of the spatial resolution. So called "spike" tests [W. Spakman and G. Nolet, in: *Mathematical Geophysics: A Survey of Recent Developments in Seismology and Geodynamics*, N. J. Vlaar *et al.*, Eds. (Reidel, Dordrecht, Netherlands, 1988)] were computed for a range of "spike" sizes between 0.6° and 6° to determine the image resolution at different spatial scales. "Layer cake" tests used synthetic input models derived from the structures recovered in the tomographic model to test lateral and vertical resolution of the recovered features.
16. E. Carminati *et al.*, *Earth Planet. Sci. Lett.* **160**, 651 (1998).
17. M. Granet and J. Trampert, *Geophys. J. Int.* **99**, 583 (1989).
18. In the upper mantle plume conduits are thought to be very narrow (50 to 300 km) (*28*), while lower mantle plumes are thought to be significantly wider (around a factor of 3 to 5 times wider than upper mantle plumes) (*26*) because of the higher viscosity of the lower mantle.
19. H. Bijwaard and W. Spakman, *Earth Planet. Sci. Lett.* **166**, 121 (1999).
20. H. Bijwaard, thesis, Utrecht University, Netherlands (1999).
21. S. Grand, R. D. van der Hilst, S. Widiyantoro, *GSA Today* **7**, 1 (1997); R. D. van der Hilst, S. Widiyantoro, E. R. Engdahl, *Nature* **386**, 578 (1997).
22. S. Goes, R. Govers, P. Vacher, *J. Geophys. Res.*, in press.
23. The excess temperatures of plumes have been estimated to be 75 to 300°C in the upper mantle and 150 to 300°C in the lower mantle (*19*, *28*).
24. S. Karato, *Geophys. Res. Lett.* **20**, 1623 (1993).
25. D. L. Anderson, *Nature* **297**, 391 (1982).
26. P. E. van Keken and C. W. Gable *J. Geophys. Res.* **100**, 20,291 (1995); V. Steinbach and D.A. Yuen, *Phys. Earth Planet. Int.* **103**, 85 (1997); T. Nakakuki, D. A. Yuen, S. Honda, *Earth Planet. Sci. Lett.* **146**, 379–391, (1997); D. A. Yuen, L. Cserepes, B. A. Schroeder, *Earth Planets Space* **50**, 1035 (1998); B. Steinberger and R. J. O'Connell, *Geophys. J. Int.* **132**, 412 (1998).
27. B. L. N. Kennett, E. R. Engdahl, R. Buland, *Geophys. J. Int.* **122**, 108 (1995).
28. R. White and D. McKenzie, *J. Geophys. Res.* **94**, 7685 (1989); N. H. Sleep, *J. Geophys. Res.* **95**, 6715 (1990); G. Ito, J. Lin, C.W. Gable, *Earth Planet. Sci. Lett.* **144**, 53 (1996); H-C. Nataf and J. C. VanDecar, *Nature* **364**, 115 (1993); J. C. VanDecar, D. E. James, M. Assumpção, *Nature* **378**, 25 (1995); C. J. Wolfe *et al.*, *Nature* **385**, 245 (1997); Y. Shen *et al.*, *Nature* **395**, 62 (1998).
29. E. Griesshaber, R. K. O'Nions, E. R. Oxburgh, *Chem. Geol.* **99**, 213 (1992); T. J. Dunai and H. Baur, *Geochim. Cosmochim. Acta* **59**, 2767 (1995).
30. We thank M. Rehkämper for discussions on the geochemical signature of plumes and two reviewers for their critical reading of our manuscript. Funding was provided by the NEESDI program (NWO grant 750-29-601) (S.G.) and the Netherlands Geoscience Foundation (GOA) (H.B.), both financially supported by the Netherlands Organization for Scientific Research (NWO), and by the Vening-Meinesz Research School of Geodynamics.

12 August 1999; accepted 27 October 1999

Transition States Between Pyramids and Domes During Ge/Si Island Growth

F. M. Ross,* R. M. Tromp, M. C. Reuter

Real-time observations were made of the shape change from pyramids to domes during the growth of germanium-silicon islands on silicon (001). Small islands are pyramidal in shape, whereas larger islands are dome-shaped. During growth, the transition from pyramids to domes occurs through a series of asymmetric transition states with increasing numbers of highly inclined facets. Postgrowth annealing of pyramids results in a similar shape change process. The transition shapes are temperature dependent and transform reversibly to the final dome shape during cooling. These results are consistent with an anomalous coarsening model for island growth.

The formation of self-assembled islands, or quantum dots, during the epitaxial growth of Ge on Si is characterized by several distinct island shapes and an unusual island size distribution. The islands form spontaneously as a means of relieving the strain caused by the mismatch between the larger Ge lattice and the smaller lattice of the Si substrate. The question of whether the islands are thermodynamically stable or only transient structures is important both for understanding the general process of semiconductor epitaxy and for developing novel quantum dot–based electronic devices requiring well-controlled arrays of islands. Island growth has therefore been studied extensively using both in situ and post-growth analytical techniques.

For Ge deposition on Si(001), islands first appear after the formation of a flat wetting layer ~3 monolayers (ML) thick. At low growth temperatures the islands are rectangular-based huts with {501} facets (*1*), whereas at higher temperatures two different island shapes exist, depending on island size (*2*). Small islands are square-based pyramids, again with {501} facets, whereas larger islands are multifaceted domes, which have a higher aspect ratio and include facets such as {113} (*3*). The same island morphology is observed, although with larger lateral dimensions, for lower-strained Ge_xSi_{1-x} alloys on Si(001) (*4*).

Detailed observations of island shapes and size distributions made using scanning tunneling microscopy (*2*, *5*) reveal interesting details of the evolution of the islands. Over a wide range of growth conditions, Ge islands show a bimodal distribution of sizes, with pyramids occupying the lower peak of the volume distribution and domes occupying the higher peak. Several models have been proposed (*2*, *5*, *6*) to explain how islands grow from low-volume pyramids to high-volume domes, and there is still much debate about which factors determine the island size distribution.

The details of the process that takes place as an island changes from a pyramid to a dome are crucial in understanding growth kinetics and in distinguishing between models. We have therefore studied island growth using low-energy electron microscopy (LEEM), a technique capable of distinguishing between different shapes and determining island sizes in real time during growth.

Our experiments were carried out in a LEEM apparatus with in situ growth capabilities, a base pressure of 2×10^{-10} torr, and a point resolution of 5 nm (*7*). Si(001) specimens were flash-cleaned and heated to the desired growth temperature of ~650° to 700°C. Ge_xSi_{1-x} was grown by chemical vapor deposition using a mixture of disilane and digermane gases introduced to the specimen area through a capillary tube. Typical growth rates, measured from the motion of steps in the early stages of growth or from post-growth cross-sectional analysis, were ~1 to 5 ML/min. Images were recorded at video rate, at electron energies of 5 to 10 eV.

In the LEEM images (Fig. 1A), pyramids are clearly distinguished by their cross-shaped pattern, whereas domes appear qualitatively different, most notably showing four bright areas each bisected by a narrow dark line. The eight bright regions, or facet beams, are only visible within a certain range of electron energy. They are formed when electrons diffracted from highly inclined facets pass through the objective aperture, and they indicate that additional facets are present on the domes; however, because of local focusing effects, the bright regions on the image may not correspond exactly to the spatial positions of the additional facets. Examination by ex situ scanning electron microscopy (Fig. 1B)

IBM T. J. Watson Research Center, Post Office Box 218, Yorktown Heights, NY 10598, USA.

*To whom correspondence should be addressed. E-mail: fmross@us.ibm.com

confirmed the presence of four extra pairs of facets on the domes and indicated that these facets were close to {518}. Because recent observations of the stability of Ge surfaces (*8*) suggest that the only stable facet close to {518} is actually {15 3 23}, we assign indices of {15 3 23} to these eight dome facets (see below). Small {113} and {501} facets are also present on the domes. It has usually been assumed that domes are bounded by {113} and {301} facets (*1–3, 9*), and it is interesting that our images show no evidence for the {301} facet.

Video-rate observation shows that each island passes through several distinct configurations during growth (Figs. 2 and 3). The earliest stage of growth is a roughening process with a characteristic length scale that depends on strain (*10*). The amplitude of the roughness increases until {501} facets appear, and a dense array of pyramids eventually forms from the rough surface (Fig. 2A). The pyramids then coarsen, undergoing a large decrease in density, and eventually change to domes as they increase in size beyond a critical diameter (Fig. 2, B and C). The transition from pyramid to dome is not accomplished suddenly but can take several minutes (Fig. 3). As an island approaches the critical diameter, its projected shape begins to change from square to circular, and facet beams appear near the rounded corners. These facet beams persist until the final dome shape is reached and are attributed to {113} facets. The overall shape at this point appears to be a pyramid that has been truncated by removal of its lowest four vertices (but not the top vertex), leaving an octagonal base, which appears almost circular in the images (TP in Fig. 3). The next stage is the appearance of contrast from one or more of the {15 3 23} facets, which gradually brightens and increases in extent. The {15 3 23} facets always appear in pairs, although one facet may be larger than the other, particularly if the original pyramid was not perfectly square or had an asymmetric neighborhood. It is interesting that each dome develops these facet pairs in its own order. Some domes pass through all the transition states (D1, D2, and D3 in Fig. 3); others may develop two, three, or even all four facet pairs simultaneously. We suppose that slight asymmetries in the local environment or the original island shape account for the exact pattern for any island. The transition shapes may persist for many minutes at the growth temperature, and growth must be continued for several hours before most of the islands have attained the D4 shape.

The evolution of the diameter and shape of representative islands (Fig. 4) gives a clearer picture of the development of an ensemble of islands, and shows the coarsening during the early stages and the later appearance of transition shapes followed by domes. The islands have one of two fates: They either reach the TP state and eventually become domes, or they shrink and disappear. The pyramids do not appear to be stable, although in some experiments they can persist through several hours of observation (as in Fig. 2): The kinetics become extremely slow as the islands coarsen and separate. As long as pyramids are present, we do not observe the disappearance of TP islands.

The time spent in the transition states can be surprisingly long. We therefore performed several experiments to see whether island development is limited by the flux of Ge and Si. Coarsening experiments, in which a population of pyramids was prepared and then annealed with no additional flux, displayed kinetics similar to those seen in the growth experiments where the flux remained on: The pyramids were not stable, and coarsening and formation of domes via transition states occurred in both cases, demonstrating that the flux is not limiting island development. During coarsening, the island number density varied with time in a way that is consistent with diffusion-limited Ostwald ripening (*11*). A quantitative verification of Ostwald ripening would require comparison of the shape of the island size distribution with theory, which is not easily done here because of the relatively small number of islands measured.

Island growth has been the subject of intense theoretical interest, and several models have been proposed to explain island development. The bimodal distribution, and particularly the lack of many islands at intermediate sizes, led Medeiros-Ribeiro *et al.* (*2*) to propose that the size distribution reflects an equilibrium state. The pyramid and dome shapes are supposed to have energy minima at two discrete volumes, and the width of the bimodal distribution about each minimum is due to thermal broadening. The transition from pyramid to dome is then a thermally excited process that overcomes the energy barrier between the pyramid and dome energy minima and involves rapid accumulation

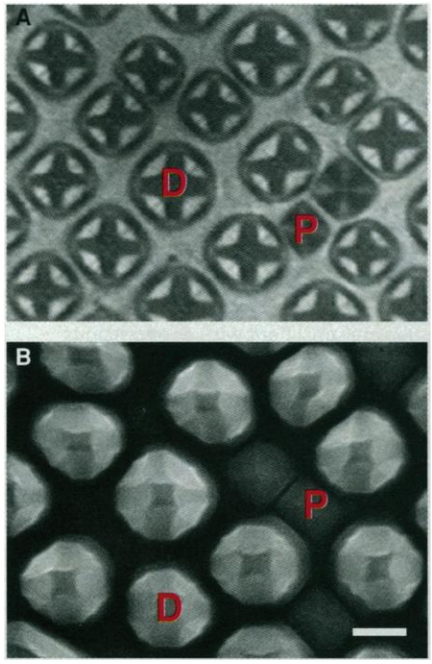

Fig. 1. (**A**) Densely packed pyramids (P) and domes (D) formed after 56 min of growth of $Ge_{0.3}Si_{0.7}$ at 710°C. Si_2H_6, He, and Ge_2H_6 gases were used in the ratio 100:10:1 and a total pressure of 1.0×10^{-5} torr, and the exact composition was calibrated after growth by means of Rutherford backscattering. The image was recorded at room temperature using bright-field imaging conditions with an electron energy of 4 eV. The {110} directions are parallel to the edges of the images. (**B**) Scanning electron micrograph of a similar specimen grown for 39 min at 690°C. The islands are faceted and ~70 nm high. The facet edges have been enhanced by filtering to enable comparison of island shapes with those in (A).

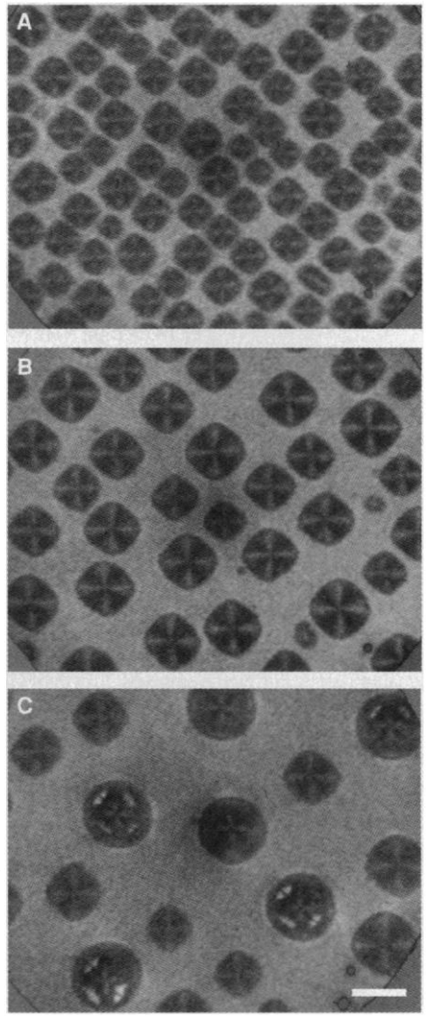

Fig. 2. Evolution of island shapes. These images were recorded during post-growth annealing of a $Ge_{0.25}Si_{0.75}$ alloy grown for 6 min at 670°C; the sequence is similar in experiments where the flux remains on, although a denser array of islands can form. Imaging conditions were identical to those of Fig. 1A. Images are shown after (**A**) 1860 s, (**B**) 3540 s, and (**C**) 22,080 s (more than 6 hours) of annealing. In (C), transition shapes with zero, two, three, and four dome facet pairs can be seen.

of 10^5 atoms. A very short time scale was suggested for this transition to account for the few islands seen with intermediate sizes. However, real-time observations of island growth in the transmission electron microscope (*6*) showed that islands actually increase in size very smoothly. Although island shapes could not be distinguished in these experiments, the data were more consistent with an anomalous coarsening model. This is a kinetic rather than a thermodynamic model, whereby islands grow by a process similar to Ostwald ripening, but with kinetics modified by an abrupt drop in chemical potential that occurs as islands grow past a critical volume and change their shape. In this model the bimodal distribution is a transient phenomenon that forms as the drop in chemical potential accelerates the coarsening of the largest islands in the distribution.

Transition states were not included in the anomalous coarsening model, but we expect that the addition of intermediate configurations will not change the qualitative pattern of the kinetics. The population of pyramids will coarsen until some islands reach the critical volume for changing to the TP shape; the chemical potential of these TP islands will drop, accelerating their growth, and the process will repeat at each transition volume (D1, D2, and D3) until the islands become domes (D4). With their high chemical potential, any remaining pyramids will shrink and disappear. We would not expect to see TP islands shrinking until all the pyramids had disappeared. Furthermore, as the islands coarsen, the kinetics are expected to become very slow. This simple model is in good agreement with our observations, whereas a slow transformation via transition states is not consistent with a thermally excited, rapid transition between equilibrium shapes (*2*).

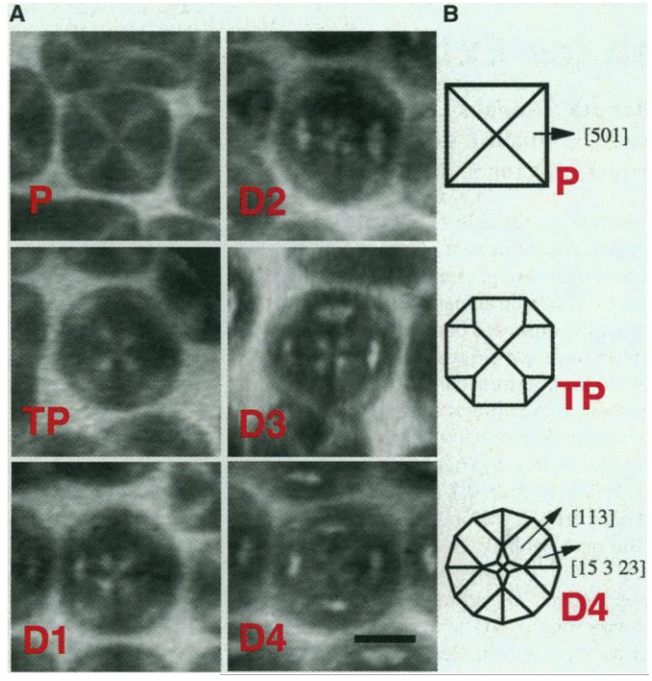

Fig. 3. (**A**) Images recorded during growth of $Ge_{0.25}Si_{0.75}$ at 730°C showing the pyramid (P), transition (TP, D1, D2, D3), and dome (D4) shapes. The (100) direction is horizontal. (**B**) Schematic diagrams showing the facets present on the P, TP, and D4 shapes. The TP shape is made up of {501} and {113} facets.

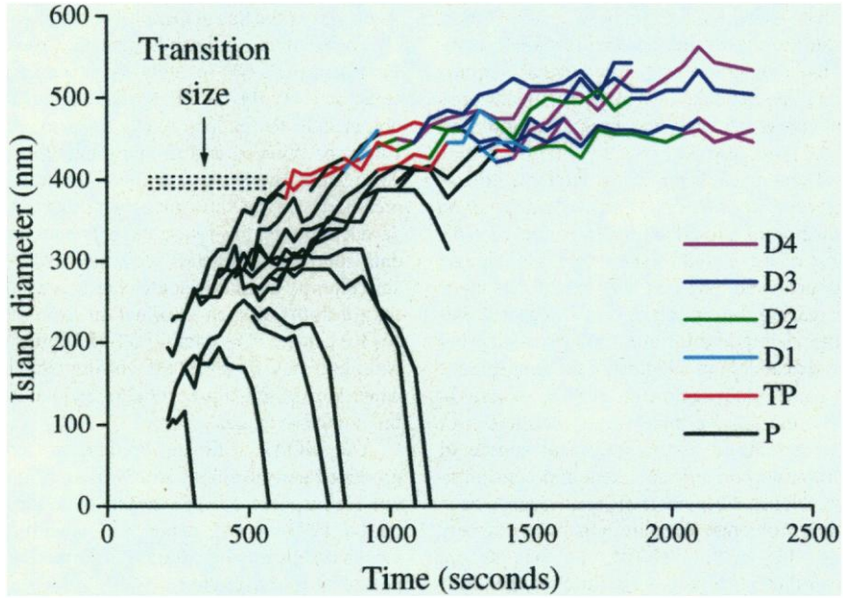

Fig. 4. Size and shape of representative islands measured during growth at 690°C with composition $Ge_{0.3}Si_{0.7}$. The island diameter was measured in the [100] direction; the color indicates the island shape. Some of the pyramids shrink to zero diameter as a result of coarsening. Trajectories ending above zero indicate islands that drifted out of the field of view.

It is interesting to consider the nature of the shape change in the anomalous coarsening model. Two-dimensional calculations (*12*) suggest that the shape transition should be first order with island size, with discontinuous introduction of steeper facets at the island edge. In three dimensions, the appearance of steeper facets at the lower vertices of the pyramids in the TP shape and then the replacement of the pyramid edges by additional facets in the D1 to D4 shapes is consistent with such a transition.

Finally, it is important to discuss why the transition shapes have not previously been observed, especially given their long lifetime. We find that cooling changes the appearance of the islands markedly, in particular altering the proportions of different island shapes. When D4 islands are cooled, the {15 3 23} dome facet contrast becomes stronger and larger in area, suggesting that these facets have increased in size. This effect can be seen by comparing D4 islands in Fig. 1A with those in Fig. 2C or Fig. 3. Furthermore, dome facet contrast appears on transitional shapes (although not pyramids) upon cooling. For example, when a specimen consisting mainly of P and TP islands was cooled from 740°C to 640°C, the percentage of P remained unchanged (at 38%), but most of the TP shapes disappeared (dropping from 36% to only 8% of the population). Dome facets had appeared on these TP shapes, increasing the proportion of D4 islands from 2% to 24% and the proportion of D1+D2+D3 islands from 24% to 30%. At room temperature, the specimen therefore appeared to consist almost entirely of pyramids and domes with few intermediate shapes. This transition was reversible, with TP shapes reappearing at higher temperatures. We suppose that the energies of all facets are temperature-dependent, and we speculate that the {15 3 23} facet becomes slightly more favorable at lower temperatures, relative to other TP facets. This result emphasizes the importance of observations made under growth conditions for understanding growth mechanisms.

References and Notes

1. Y.-W. Mo, D. E. Savage, B. S. Swartzentruber, M. G. Lagally, *Phys. Rev. Lett.* **65**, 1020 (1990).
2. G. Medeiros-Ribeiro, A. M. Bratkovsky, T. I. Kamins, D. A. A. Ohlberg, R. S. Williams, *Science* **279**, 353 (1998).
3. T. I. Kamins, E. C. Carr, R. S. Williams, S. J. Rosner, *J. Appl. Phys.* **81**, 211 (1997); M. Tomitori, K. Watanabe, M. Kobayashi, O. Nishikawa, *Appl. Surf. Sci.* **76–77**, 322 (1994).
4. J. A. Floro *et al.*, *Phys. Rev. B* **59**, 1990 (1999).
5. T. I. Kamins, G. Medeiros-Ribeiro, D. A. A. Ohlberg, R. S. Williams, *J. Appl. Phys.* **85**, 1159 (1999).
6. F. M. Ross, J. Tersoff, R. M. Tromp, *Phys. Rev. Lett.* **80**, 984 (1998).
7. R. M. Tromp, M. Mankos, M. C. Reuter, A. W. Ellis, M. Copel, *Surf. Rev. Lett.* **5**, 1189 (1998).
8. Z. Gai, X. Li, R. G. Zhao, W. S. Yang, *Phys. Rev. B* **57**, 15060 (1998).
9. M. Goryll, L. Vescan, K. Schmidt, S. Mesters, H. Luth, *Appl. Phys. Lett.* **71**, 410 (1997); M. A. Lutz, R. M. Feenstra, P. M. Mooney, J. Tersoff, J. O. Chu, *Surf. Sci.* **316**, L1075 (1994).
10. R. M. Tromp, F. M. Ross, M. C. Reuter, in preparation.
11. M. Zinke-Allmang, L. C. Feldman, M. Grabow, *Phys. Rev. B* **39**, 7848 (1989).
12. I. Daruka, J. Tersoff, A.-L. Barabasi, *Phys. Rev. Lett.* **82**, 2753 (1999).
13. We thank K. Pope for Rutherford backscattering analysis and J. Tersoff for helpful discussions.

22 July 1999; accepted 20 October 1999

Global Warming and Northern Hemisphere Sea Ice Extent

Konstantin Y. Vinnikov,[1]* Alan Robock,[2] Ronald J. Stouffer,[3] John E. Walsh,[4] Claire L. Parkinson,[5] Donald J. Cavalieri,[5] John F. B. Mitchell,[6] Donald Garrett,[7] Victor F. Zakharov[8]

Surface and satellite-based observations show a decrease in Northern Hemisphere sea ice extent during the past 46 years. A comparison of these trends to control and transient integrations (forced by observed greenhouse gases and tropospheric sulfate aerosols) from the Geophysical Fluid Dynamics Laboratory and Hadley Centre climate models reveals that the observed decrease in Northern Hemisphere sea ice extent agrees with the transient simulations, and both trends are much larger than would be expected from natural climate variations. From long-term control runs of climate models, it was found that the probability of the observed trends resulting from natural climate variability, assuming that the models' natural variability is similar to that found in nature, is less than 2 percent for the 1978–98 sea ice trends and less than 0.1 percent for the 1953–98 sea ice trends. Both models used here project continued decreases in sea ice thickness and extent throughout the next century.

The cryosphere is an important component of climate because of its effect on Earth's surface albedo (*1*) and its role in reducing the amount of heat exchanged between the atmosphere and the ocean (or land) beneath the ice. In particular, sea ice extent has long been recognized as an important indicator of the state of the climate system in observational and modeling studies. Early simulations of changes in sea ice coverage and sea ice thickness associated with global warming showed large sea ice reductions (*2*, *3*), but these simulations were not compared with observations. Observations now span a sufficiently long period to show a substantial decrease of Northern Hemisphere (NH) sea ice during the past few decades. Here, we use sea ice extent in an attempt to detect recent global climate change and examine whether it might be attributable to anthropogenic causes by comparing it with model-calculated global warming trends and trendlike low-frequency fluctuations that appear randomly in very long control runs of the same models.

There have been many attempts to use observed trends in NH sea ice extent as an indicator of global climate change (*4–16*). Most of these studies show that, on average, the observed NH sea ice extent has been decreasing during the past few decades. Satellite visible and infrared images, which became available in 1966, were the first sources of global information on sea ice extent. In 1972, the passive microwave satellite sensor was introduced as an additional source of information on sea ice extent and concentration. Nonsatellite observational records have many problems; they are generally not very long, they are not global, and they do not cover the entire year. Very little sea ice cover data are currently available for 1941–45.

We used the following five sources of observations to determine sea ice extent in the NH: the University of Illinois sea ice group, the Russian Arctic and Antarctic Research Institute, the NOAA Climate Prediction Center, the Norwegian Nansen Environmental and Remote Sensing Center, and the NASA Goddard Space Flight Center.

The University of Illinois sea ice group has just revised and updated its data set (*6*, *13*). The most reliable data cover the period since 1953. The recent inclusion of data from the Norwegian Polar Institute added data for the winter months of the 1901–52 period. For the period from 1972 to the present, the primary data source was the digital version of the U.S. National Ice Center (NIC) chart series. The NIC charts, in turn, draw on satellite passive microwave imagery [including the period of continuous coverage by a scanning multichannel microwave radiometer (SMMR) and a special sensor microwave imager (SSM/I) from 1978 to the present], together with other available data from visible and infrared satellite sensors and from any near–real-time aircraft reconnaissance and surface reports. Sea ice extent at the end of each month is estimated as the total ocean area poleward of the sea ice boundary, not taking into account information about its concentration. The averaging domain does not include the Baltic, Caspian, Aral, Black, or Azov seas or the Sea of Okhotsk south of 45°N.

The Russian Arctic and Antarctic Research Institute reports NH monthly mean sea ice extents for 1960–90 (*5*). The spatial domain does not include the Baltic, Azov, Caspian, Aral, Black, or White seas. Ice concentration is not considered. The Russian sea ice data draw increasingly on satellite imagery during recent decades. During the 1960s, the only substantial data sources were aerial reconnaissance and ship reports, including some charts or syntheses (or both) of such information from other sea ice centers. The data for all 12 months are complete only for 1972–90; earlier data have gaps that do not allow reliable estimates of the annual averages.

The NOAA Climate Prediction Center produced end-of-month Northern and Southern Hemisphere sea ice extent data for the period 1973–94 (*8*), using NIC weekly sea ice charts. Ice concentration information is not taken into account.

The Norwegian Nansen Environmental and Remote Sensing Center used passive microwave satellite observations to measure 1978–94 sea ice extent in the latitudinal belt

[1]Department of Meteorology, University of Maryland, College Park, MD 20742, USA. [2]Department of Environmental Sciences, Rutgers—The State University of New Jersey, 14 College Farm Road, New Brunswick, NJ 08901–8551, USA. [3]Geophysical Fluid Dynamics Laboratory, National Oceanic and Atmospheric Administration (NOAA), Post Office Box 308, Princeton, NJ 08542, USA. [4]Department of Atmospheric Sciences, University of Illinois, 105 South Gregory Street, Urbana, IL 61801, USA. [5]Code 971, Oceans and Ice Branch, NASA Goddard Space Flight Center, Greenbelt, MD 20771, USA. [6]Hadley Centre for Climate Prediction and Research, Meteorological Office, Bracknell, RG12 2SZ, UK. [7]Climate Prediction Center, National Weather Service, National Centers for Environmental Prediction, NOAA, 5200 Auth Road, Room 800, Camp Springs, MD 20746, USA. [8]Arctic and Antarctic Research Institute, 38 Bering Street, St. Petersburg 199397, Russia.

*To whom correspondence should be addressed. E-mail: kostya@atmos.umd.edu

References and Notes

[2] **Shape Transition of Germanium Nanocrystals on a Silicon (001) Surface from Pyramids to Domes**

Gilberto Medeiros-Ribeiro; Alexander M. Bratkovski; Theodore I. Kamins; Douglas A. A. Ohlberg; R. Stanley Williams

Science, New Series, Vol. 279, No. 5349. (Jan. 16, 1998), pp. 353-355.

Stable URL:

http://links.jstor.org/sici?sici=0036-8075%2819980116%293%3A279%3A5349%3C353%3ASTOGNO%3E2.0.CO%3B2-1